

# Hippocampal blood–brain barrier permeability is related to the APOE4 mutation status of elderly individuals without dementia

Journal of Cerebral Blood Flow & Metabolism  
2021, Vol. 41(6) 1351–1361  
© The Author(s) 2020  
Article reuse guidelines:  
sagepub.com/journals-permissions  
DOI: 10.1177/0271678X20952012  
journals.sagepub.com/home/jcbfm



Won-Jin Moon<sup>1</sup> , Changmok Lim<sup>1</sup> , Il Heon Ha<sup>1</sup>,  
Yeahoon Kim<sup>1</sup>, Yeonsil Moon<sup>2</sup>, Hee-Jin Kim<sup>3</sup> and  
Seol-Heui Han<sup>2</sup>

## Abstract

Blood–brain barrier (BBB) disruption, modulated by APOE4 mutation, is implicated in the pathogenesis of cognitive decline. We determined whether BBB permeability differed according to cognitive functioning and APOE4 status in elderly subjects without dementia. In this prospective study, 33 subjects with mild cognitive impairment (MCI) and 33 age-matched controls (normal cognition [NC]) underwent 3 T brain magnetic resonance imaging. The Patlak model was used to calculate tissue permeability ( $K_{trans}$ ). A region-of interest analysis of  $K_{trans}$  was performed to compare relevant brain regions. Effects of  $K_{trans}$  on cognitive functioning were evaluated with linear regression analysis adjusted for confounding factors. NC and MCI groups did not differ in terms of vascular risk factors or hippocampal  $K_{trans}$ , except for hippocampal volume. Hippocampal  $K_{trans}$  was significantly higher in APOE4 carriers than in non-carriers ( $p = 0.007$ ). Factors which predicted cognitive functioning included hippocampal volume ( $\beta = -0.445$ , standard error [SE] = 0.137,  $p = 0.003$ ) and hippocampal BBB permeability ( $\beta = 0.142$ , SE = 0.050,  $p = 0.008$ ) after correcting for age, education, and APOE4 status. This suggests that hippocampal BBB permeability is associated with APOE4 mutation, and may predict cognitive functioning. BBB permeability imaging represents a distinct imaging biomarker for APOE4 mutations in NC and MCI subjects and for determining the degree of APOE4-related pathology.

## Keywords

Alzheimer's disease, APOE4, blood–brain barrier, dementia, permeability

Received 15 March 2020; Revised 22 July 2020; Accepted 25 July 2020

## Introduction

Alzheimer's disease (AD) is the most common type of dementia and is characterized by pathological amyloid and tau deposition. The involvement of vascular pathology in AD pathogenesis has become increasingly clear.<sup>1</sup> Accumulating evidence shows that vascular involvement in AD pathogenesis is not limited to visible large and/or small vessel pathology but extends to the level of the neurovascular unit or the blood–brain barrier (BBB).<sup>2,3</sup> BBB breakdown due to disruption of tight junctions, altered transport of molecules between the blood and the brain, aberrant angiogenesis, vessel regression, brain hypoperfusion, and inflammatory processes may initiate and/or contribute to progressive synaptic and neuronal dysfunction and neurodegenerative disorders.<sup>4</sup> Dysfunctional BBB transport can lead

to a dysregulated efflux of amyloid protein, causing toxic amyloid accumulation in the brain.<sup>5</sup>

Apolipoprotein E4 (APOE4) mutation significantly influences the development of AD.<sup>6</sup> APOE, a polymorphic

<sup>1</sup>Department of Radiology, Konkuk University Medical Center, Konkuk University School of Medicine, Seoul, Korea

<sup>2</sup>Department of Neurology, Konkuk University Medical Center, Konkuk University School of Medicine, Seoul, Korea

<sup>3</sup>Department of Neurology, Hanyang University Medical Center, Hanyang University College of Medicine, Seoul, Korea

### Corresponding author:

Won-Jin Moon, Department of Radiology, Konkuk University Medical Center, Konkuk University School of Medicine, 120-1, Neungdong-ro, Hwayang-dong, Gwangjin-gu, Seoul 05030, Korea South.  
Email: mdmoonwj@kuh.ac.kr

protein involved in cholesterol transport, has three isoforms, namely, E2, E3, and E4. The APOE4 allele is closely correlated with vascular risk factors and amyloid accumulation in AD. APOE4 is also implicated in BBB disruption.<sup>5,7</sup>

BBB permeability changes have been extensively investigated in dementia.<sup>5,8,9</sup> Traditionally, the cerebrospinal fluid (CSF)-serum albumin index is used to indicate BBB leakage in human studies.<sup>10</sup> However, the albumin index is not useful for assessing subtle BBB leakage as albumin itself is a relatively large molecule (66.5 kDa). In contrast, dynamic contrast-enhanced (DCE) magnetic resonance imaging (MRI) uses a gadolinium-based contrast agent of a relatively small molecular weight and is thus more appropriate for measuring the presence and distribution of subtle BBB leakage.<sup>11</sup> Several DCE-imaging studies of AD and mild cognitive impairments (MCIs) have been published, but detailed analyses of anatomical distribution are rare.<sup>12,13</sup>

We aimed to evaluate BBB permeability changes in patients with MCI and normal controls, and hypothesized that increased BBB permeability would follow either the anatomical pattern of common microvascular pathology (white matter) or AD-specific tau pathology (hippocampus, inferior temporal gyrus) or amyloid pathology (orbitofrontal cortex) based on previous findings.<sup>2,14</sup> We also hypothesized that BBB permeability would be increased in both patients with MCI and controls depending on the APOE mutation status, given the effects of APOE on BBB structural integrity and the functional regulation of transport proteins.<sup>5,7</sup> This prospective study thus aimed to (1) evaluate the BBB permeability of normal controls and patients with MCI and (2) evaluate differences in BBB permeability according to APOE4 status.

## Material and methods

### *Standard protocol approvals, registrations, and patient consent*

This prospective study was approved by the Institutional Review Boards of Konkuk University Medical Center (no. KUH1140118 and no. KUH1140130) and Hanyang University Medical Center (no. 2018-06-020-001). The conduct of the study was governed by ethical standards according to the Helsinki Declaration of 1975 (and as revised in 1983). Written informed consent was obtained from all participants.

### *Study participants*

In total, 106 elderly participants without dementia were consecutively enrolled from a prospective observation trial between June 2017 and May 2019. All participants

were enrolled from two different institutions and were referred to the imaging center at Konkuk University Medical Center to undergo MRI examination, including BBB permeability imaging protocols.

Of the 106 participants, we excluded one person who had a lack of basic clinical information and two people with loss of imaging data and inadequate image acquisition. Finally, a total of 103 participants were considered, comprising 44 cognitively normal (11 men, mean age  $\pm$  standard deviation:  $64.1 \pm 6.5$  years) individuals and 59 subjects with MCI (21 men;  $69.9 \pm 7.6$  years). Given the large age gap between the groups, we randomly selected 33 age-matched normal controls and 33 subjects with MCI after an age-matching procedure. The age-matching procedure was done using case-control matching in MedCalc with a maximum allowable difference of one year.

### *Clinical assessment*

We assessed all available patient information, including basic demographic characteristics, education, other medical conditions, global cognitive assessment scores (such as the Mini-Mental Status Examination (MMSE) score and clinical dementia rating sum of boxes [CDR-SB]), apolipoprotein E genotyping, and brain imaging.

Laboratory test results were used to exclude other medical conditions associated with dementia-like symptoms.<sup>15</sup> Vascular risk factors were selected based on a previous study.<sup>15</sup> The total vascular risk burden was determined by the sum of the following factors: diabetes (defined by a previous diagnosis of diabetes mellitus or as the patient currently taking any antidiabetic drug), hypertension (defined by a diagnostic history of hypertension or as the patient currently taking any antihypertensive medication), dyslipidemia (defined by a previous diagnosis of hyperlipidemia or as the patient currently taking any lipid-lowering medication), history of smoking or current smoking, cardiovascular disease history (defined by a previous diagnosis of ischemic heart disease, such as myocardial infarction, angina, symptoms of intermittent claudication or atrial fibrillation), and minor stroke history (defined by a previous diagnosis of minor stroke or transient ischemic attack).

Diagnoses of MCI were based on the Diagnostic and Statistical Manual of Mental Disorders (4th ed.) and the National Institute of Neurological and Communicative Disorders and Stroke and the Alzheimer's Disease and Related Disorders Association (NINCDS-ADRDA)<sup>16</sup> according to criteria suggested by Petersen et al.<sup>17</sup>

### *APOE genotyping*

Genomic DNA was isolated and purified using the QIA symphony DSP DNA Mini Kit (Qiagen GmbH,

Hilden, Germany) on an automated QLA symphony SP system (Qiagen) according to the manufacturer's instructions. APOE genotyping was performed using a Real-Q APOE genotyping kit (Biosewoom, Seoul, Korea) on a CFX96 Real-Time PCR Detection System (Bio-Rad, Hercules, CA, USA) according to the manufacturer's instructions. The presence of one or two copies of an APOE4 allele was defined as an APOE4 carrier.

### **MRI acquisition**

All participants underwent 3.0T brain MRI (Siemens Skyra, Siemens) using the same scanner with a 20-channel coil. The MR imaging protocol included three-dimensional (3D) T1-weighted images, 3D fluid-attenuated inversion recovery (FLAIR) images, and 3D susceptibility-weighted images (SWI). Specific parameters are provided in Supplementary Table 1.

### **DCE MRI**

For DCE imaging, a coronal 3D DCE-sequence was obtained with a dynamic series of 60 individual scans with the following parameters: repetition time (TR) = 3.10 ms, echo time (TE) = 1.04 ms, flip angle = 10°, average = 1, field-of-view = 225 × 240 mm, slice thickness = 3 mm, matrix = 180 × 192, voxel size = 1.25 × 1.25 × 3 mm with an acquisition time of 10 min and time resolution of 10 s. A pre-contrast T1-weighted gradient echo series (TR = 3.10 ms, TE = 0.97 ms) with six different flip angles (2–12°) were obtained to generate T1 mapping.<sup>11,18</sup> A standard dose of gadobutrol (0.1 mol/kg body weight; Bayer Healthcare) followed by a 30 mL saline flush was automatically injected using an injector. Injections started after the fourth dynamic scan at a flow rate of 2 mL/s.

Our DCE MRI protocol was devised according to the recommended parameters.<sup>11</sup> The acquisition time of 10 min was determined based on the trade-off between patient compliance and adequate acquisition time for permeability modeling. The acquisition plane for coronal DCE imaging data was perpendicular to the anterior commissure-posterior commissure line. The anterior and posterior boundaries of the coronal plane were the anterior and the posterior ends of the corpus callosum, which is approximately 90 mm (30 slices).

### **Structural MRI analysis**

For qualitative analysis, a neuroradiologist with 22 years of experience assessed the vascular lesion using MRI. Lacunes were defined as small lesions that were hypointense on T1-weighted images, hyperintense on T2-weighted images, and had perilesional halos on FLAIR images.<sup>19</sup> Microbleeds were defined

as a small signal void with associated blooming on T2\*-weighted SWI. The presence and number of lacunes and microbleeds were recorded as described previously.<sup>19</sup>

For assessment of white matter hyperintensity (WMH) and hippocampal atrophy, we quantified the volumes ( $\times 10^3$  mm<sup>3</sup>) for WMH on 3D FLAIR images and hippocampal volumes on 3D MPRAGE images using a clinically available software Inbrain (MIDAS Information Technology Co., Ltd) (<https://www.inbrain.co.kr/index.html>) based on the following algorithm.<sup>20</sup>

WMH volumes on 3D FLAIR images were calculated using an automatic segmentation method, as described previously.<sup>21,22</sup> A WMH candidate region mask was generated on 3D T1 images. FLAIR images were subjected to non-uniformity correction, intensity normalization, and co-registration of FLAIR and T1 images of each subject. WMH was segmented using the FMRIB Automatic Segmentation Tool (FAST) algorithm with a WMH candidate region mask on FLAIR images. By using an intensity substitution method, T1 images could be classified into white matter and gray matter. After regional parcellation, WMH volume was quantified. We used the normalized total WMH volume (nWMH volume) defined as the ratio of the WMH volume to the total intracranial volume in the following analysis.

Hippocampal volumetry was performed using automatic volumetric segmentation method based on the Freesurfer 6.0 platform.<sup>23,24</sup> The processing of volumetry was as follows: analysis failure prediction; intensity normalization; brain extraction; registration into the volume and surface atlas; white matter segmentation; white matter surface smoothing; topology correction; pial and white matter surface optimization; comparisons between output results and the database; and analysis quality management. Finally, the volume of the hippocampus was obtained. A deep learning algorithm was applied to the multiple steps, including analysis failure prediction, brain extraction, white matter segmentation, and analysis quality management to enhance the quality of the segmentation results<sup>20</sup> (Supplementary Methods). We also calculated the normalized hippocampal volume defined as the ratio of the hippocampal volume to the total intracranial volume for use in the following analysis.

### **DCE MRI analysis**

Postprocessing and region of interest (ROI) placement of DCE imaging data were performed using NordiciCE software (Version 4.1.3, NordicNeuroLab, Bergen, Norway). We used a Patlak permeability model for BBB permeability calculation. 3D T1-volume imaging

was used for structural imaging reference. The analysis was performed by a trained researcher (with three years of experience) who was blinded to the clinical diagnosis, under the supervision of an expert neuroradiologist. The vascular input function was obtained from the superior sagittal sinus using the semiautomatic method in Nordic ICE. For the Patlak model, the superior sagittal sinus is a good approximation to the vascular input function (VIF) and the choice of a large venous sinus can minimize partial volume artifacts due to the smaller diameter of the arterial lumen.<sup>11</sup> We selected the Patlak model as it is the optimal model for low-leakage conditions.<sup>11</sup> Accordingly, we obtained  $K_{\text{trans}}$  ( $\text{min}^{-1}$ ), which indicates the permeability surface area product, i.e. the volume transfer constant between the plasma and extravascular extracellular space. We also obtained  $V_p$ , which denotes the capillary blood plasma volume fraction in tissue and is expressed as a percentage.

Co-registration between the 3D T1-weighted images and parametric maps from the DCE MRI was automatically performed using a mutual information-based algorithm to search an optimal rigid transformation that aligns the two datasets.<sup>25</sup> For co-registration, coronal-reformatted 3D T1-weighted images from the original sagittal data were used, which gives more accurate co-registration between 3D T1-weighted images and DCE MRI. Eight ROIs were manually drawn on the 3D T1-weighted images and transferred to the co-registered  $K_{\text{trans}}$  map for analysis. The eight ROIs included the frontoparietal white matter (WM), cingulate WM, temporal WM, and the hippocampus in both hemispheres. For the AD-specific pathology area, we selected the hippocampus, and for the common microvascular pathology, we selected the frontoparietal, cingulate, and temporal WM. We carefully ensured that the ROIs did not include WM hyperintensity or lacunes. For the hippocampus, polygonal-shaped ROIs were used to avoid the inadvertent inclusion of adjacent vessels or CSF structures. For other regions, circular ROIs were used. Coronal slices for ROI placement were selected at the level of the interpeduncular cistern of the midbrain, which corresponded to the hippocampal body (Supplementary Figure 1). For inter-observer agreement evaluation, a neuroradiologist independently performed an ROI analysis of both hippocampi. The average size of the hippocampal ROI was  $28.7 \pm 5.4 \text{ mm}^2$ .

For deep gray matter and the cortical region, we used the ROIs that were originally extracted from the automatic segmentation software, as described above.<sup>20</sup> (Supplementary Figure 1) The volumes of regional brain structures of interest were extracted based on the Desikan Killiany atlas and subcortical atlases as described elsewhere.<sup>26</sup> Each ROI was evaluated by a neuroradiologist for its accuracy and

manually edited if a non-brain or non-target area was included. The inferior temporal gyrus, lateral orbitofrontal cortex, caudate nucleus, putamen, globus pallidus, and thalamus on both sides were chosen for the analysis. We chose the inferior temporal gyrus and lateral orbitofrontal cortex specifically because the inferior temporal gyrus is associated with early tau pathology, while the lateral orbitofrontal cortex is associated with early amyloid pathology.<sup>27,28</sup>

### Statistical analysis

Statistical analyses were performed using the Statistical Package for the Social Sciences (Version 24.0 for Windows; SPSS, Chicago, Ill) and MedCalc (Version 19.1). Differences with a  $p < 0.05$  were considered statistically significant. To compare clinical and radiological features, an unpaired  $t$ -test or Mann–Whitney  $U$  test was used for continuous variables, and a Chi-square test or Fisher's exact test was used for categorical variables. We transformed CDR-SB data using a logarithmic transformation because the variable was not normally distributed, as indicated by the normality test (i.e. the Kolmogorov–Smirnov test). Group comparisons were performed using an analysis of covariance, corrected for age, sex, education, vascular risk burden, and the normalized hippocampal volume.

Associations between CDR-SB, as a cognitive functioning score, and clinical and imaging variables were evaluated using univariate and multivariate linear regression analyses. For multivariate analysis, potential confounding variables were selected based on associations ( $p < 0.2$ ) in the univariate linear regression analysis and clinical significance. The inter-rater reliability of the ROI analysis for  $K_{\text{trans}}$  agreement was determined between two raters by calculating the intraclass coefficient with a two-way mixed-effects model using absolute agreement and average measurements.

## Results

The clinical characteristics, including education status and vascular risk burden, of participants with normal cognition (NC) and with MCI are presented in Table 1.

### BBB permeability and the presence of MCI in elderly participants without dementia

No significant difference in vascular risk burden was observed between the NC and MCI groups ( $p = 0.398$ ). However, cognitive functioning, such as CDR-SB scores ( $p < 0.001$ ) and education status ( $p = 0.005$ ), differed between the groups.

The structural MRI analysis did not reveal any significant differences in any of the vascular disease MRI

**Table 1.** Clinicodemographic and imaging characteristics of the total population ( $n = 66$ ).

Characteristic	Control ( $n = 33$ )	MCI ( $n = 33$ )	$p$ value
Age, years	65.7 ± 6.4	65.9 ± 6.6	0.895
Female	22 (66.7%)	21 (63.6%)	0.796
APOE4 carrier	3/11 (27.2%)	14/24 (58.3%)	0.146
Education, years	12.3 ± 3.8	9.6 ± 3.7	0.005*
MMSE	28.0 ± 1.7	26.1 ± 3.0	0.003*
CDR-SB	0.364 ± 0.359	1.401 ± 0.879	<0.001*
Vascular risk burden	1.36 ± 1.25	1.70 ± 1.49	0.398
WMH volume ( $\times 10^3$ mm <sup>3</sup> )	9.385 ± 11.735	6.862 ± 5.610	0.269
Hippocampus volume ( $\times 10^3$ mm <sup>3</sup> )	3.988 ± 0.428	3.612 ± 0.523	0.002*
nWMH volume ( $\times 10^{-3}$ )	5.896 ± 7.007	4.592 ± 3.785	0.351
nHippocampus volume ( $\times 10^{-3}$ )	1.275 ± 0.149	1.180 ± 0.179	0.030*
Lacunae ( $n$ )	0.0 ± 0.0	0.3 ± 0.9	0.154
Microbleeds ( $n$ )	0.4 ± 1.7	1.7 ± 4.1	0.733

Note: Data are presented as the  $n$  (%) or as the mean ± standard deviation.

MMSE: Mini-mental State Examination; CDR-SB: clinical dementia rating sum of boxes; WMH: white matter hyperintensity; nWMH volume: normalized WMH volume, defined as the ratio of the WMH volume to the total intracranial volume; nHippocampus volume: normalized Hippocampus volume, defined as the ratio of the hippocampus volume to the total intracranial volume.

\* $p < 0.05$ .

findings (lacunes, microbleeds, and nWMH volumes). Normalized hippocampal volume was significantly lower in subjects with MCI than in subjects with NC ( $p = 0.030$ ) (Table 1).

The permeability rate of the BBB ( $K_{\text{trans}}$ ,  $10^{-3} \text{ min}^{-1}$ ) of the left caudate nucleus was higher in subjects with MCI than in subjects with NC ( $p = 0.016$ ). However,  $K_{\text{trans}}$  was not significantly different between the age-matched groups for any of the other brain regions that were assessed, including the hippocampus (Figure 1). Also, there were no differences in  $V_p$  across brain regions between the two groups. Comparisons of each region are presented in Supplementary Table 2.

### BBB permeability and APOE4 mutation status

In our subgroup analysis based on the APOE4 status (positive = 17; negative = 18), no significant differences in MCI diagnosis ( $p = 0.088$ ), CDR-SB score ( $p = 0.201$ ), or vascular risk burden ( $p = 0.363$ ) were observed (Table 2). APOE4 carriers and non-carriers did not differ in terms of the nWMH volume ( $p = 0.099$ ), lacunae ( $p = 0.563$ ), or microbleeds ( $p = 0.634$ ) (Table 1). Furthermore, the normalized hippocampal volume did not differ between APOE4 carriers and non-carriers ( $p = 0.122$ ) (Table 2).

The BBB permeability rate of the hippocampus was significantly higher ( $p = 0.007$ ) in the APOE4 carrier group ( $K_{\text{trans}} = 0.790 \pm 0.512 \times 10^{-3} / \text{min}$ ) than in the non-carrier group ( $K_{\text{trans}} = 0.406 \pm 0.339 \times 10^{-3} / \text{min}$ ), even after correcting for age, sex, education, vascular risk burden, and hippocampal atrophy. The trend of higher BBB permeability in the presence of APOE4

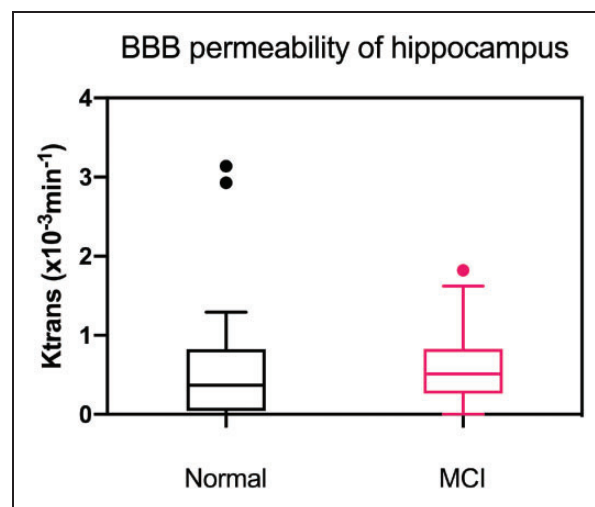


**Figure 1.** Differences in regional BBB permeability ( $K$ ) of the hippocampus by cognitive status in the total population ( $n = 66$ ). Note there was no statistically significant difference in hippocampal  $K_{\text{trans}}$  between the two groups. Dots denote the outliers. BBB: blood brain barrier.

persisted in both NC and MCI subjects (Figures 2 and 3). BBB permeability was not significantly different between the groups in the other cortical, deep gray matter, and white matter regions that were analyzed (Supplementary Table 3).

Regarding  $V_p$ , the APOE4 carrier group showed significantly lower  $V_p$ s in the inferior temporal gyrus ( $2.669 \pm 0.913\%$  vs.  $3.523 \pm 1.443\%$ ,  $p = 0.003$ ), globus pallidus ( $1.251 \pm 0.676\%$  vs.  $1.796 \pm 1.021\%$ ,  $p = 0.005$ ), and temporal WM ( $2.951 \pm 2.249\%$  vs.

**Table 2.** Clinical and imaging characteristics of the subgroup with known APOE4 status ( $n = 35$ ).

Characteristic	APOE4 (-) ( $n = 18$ )	APOE4 (+) ( $n = 17$ )	$p$ value
Age, years	65.2 ± 7.08	66.8 ± 6.25	0.494
MCI	10 (55.6%)	14 (82.4%)	0.088
APOE alleles	23/33 (1/17)	34/44 (13/4)	NA
Female	11 (51.1%)	7 (41.2%)	0.318
Education, years	12.0 ± 3.89	10.5 ± 4.4	0.288
MMSE	27.7 ± 1.9	26.7 ± 3.4	0.283
CDR-SB	0.941 ± 0.864	1.294 ± 3.445	0.201
Vascular risk burden	1.72 ± 1.01	2.18 ± 1.81	0.363
WMH volume ( $\times 10^3$ mm <sup>3</sup> )	1.47 ± 1.00	1.52 ± 1.00	0.865
Hippocampus volume ( $\times 10^3$ mm <sup>3</sup> )	0.52 ± 0.79	0.97 ± 0.73	0.114
nWMH volume ( $\times 10^{-3}$ )	0.53 ± 0.80	1.00 ± 0.79	0.099
nHippocampus volume ( $\times 10^{-3}$ )	0.53 ± 0.80	0.94 ± 0.74	0.122
Lacunae ( $n$ )	0.0 ± 0.0	0.1 ± 0.3	0.563
Microbleeds ( $n$ )	4.7 ± 15.0	1.4 ± 3.6	0.634

MMSE: Mini-mental State Examination; CDR-SB: clinical dementia rating sum of boxes; WMH: white matter hyperintensity; APOE: apolipoprotein E; nWMH: normalized total WMH volume; nHippocampus: normalized hippocampus volume; MCI: mild cognitive impairment.

Note: Data are presented as the  $n$  (%) or as the mean ± standard deviation.

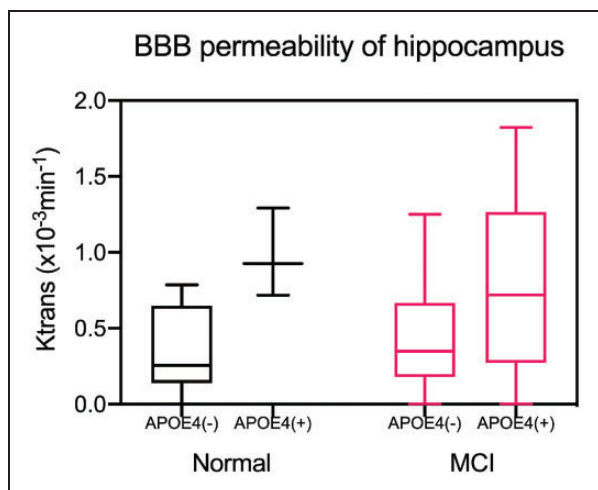


**Figure 2.** Differences in regional BBB permeability according to APOE4 status and cognitive status in the subgroup with a known APOE4 status ( $n = 35$ ). BBB: blood brain barrier. The BBB permeability rate of the hippocampus was significantly higher in the APOE4 carrier group ( $n = 17$ ) than in the non-carrier group ( $n = 18$ ), even after correcting for age, sex, education, vascular risk burden, and hippocampal atrophy.

3.590 ± 2.639%,  $p = 0.021$ ) compared with the non-carrier group.

### Correlation between BBB permeability and cognitive functioning score

In the total population ( $n = 66$ ), univariate and multivariate regression analyses were performed to predict cognitive functioning assessed by CDR-SB. Age, education, vascular risk burden, nWMH volume, and  $K_{trans}$  of the hippocampus were not correlated with

CDR-SB. Only normalized hippocampal volume correlated with CDR-SB in the univariate analysis ( $p = 0.002$ ). The multivariate analysis revealed that both normalized hippocampal volume and education were the only predictive factors for CDR-SB ( $F = 3.578$ ,  $p = 0.004$ ) (Table 3).

The results differed when the analysis was restricted to subjects with a known APOE status. Univariate and multivariate regression analyses were performed using the covariates (age, education, APOE status, vascular risk burden, nWMH volume, and normalized hippocampal volume) to predict cognitive function assessed by CDR-SB. The valuable predictive factors were  $K_{trans}$  of the hippocampus and  $V_p$  of the inferior temporal gyrus, as well as normalized hippocampal volume and education ( $F = 3.821$ ,  $p = 0.004$ ) (Table 4). Forward stepwise analysis, however, showed that  $K_{trans}$  of hippocampus and normalized hippocampal volume were the only two predictors of CDR-SB ( $F = 9.559$ ,  $p = 0.001$ ) (Table 4).

### Inter-observer reliability of the $K_{trans}$ measurement

Inter-observer reliabilities of the  $K_{trans}$  measurements for the right and left hippocampi had intraclass correlation coefficients of 0.908 (95% confidence interval [CI]: 0.794 to 0.959) and 0.916 (95% CI: 0.812 to 0.963), respectively.

### Discussion

The study demonstrated that BBB permeability did not differ according to the presence of MCI in either the regional white or gray matter, or in the hippocampus. However, in the subgroup with a known APOE4

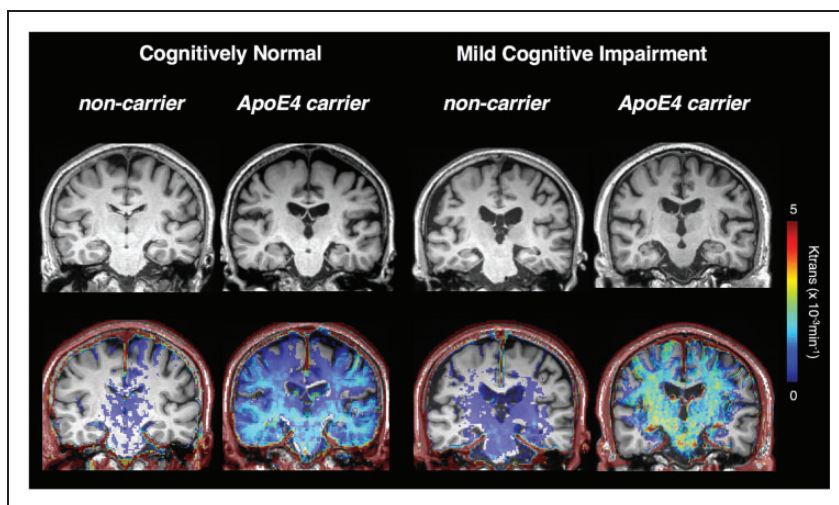


**Figure 3.** Exemplary cases of BBB permeability imaging ( $K_{trans}$  map) by APOE4 and cognitive status. BBB: blood brain barrier. The trend of higher BBB permeability in the presence of APOE4 persisted in both cognitive normal and MCI subjects.

**Table 3.** Predictors of CDR-SB in the total population ( $n = 66$ ).

Independent variable	Univariable regression			Multivariable regression (enter)		
	B	SE	p value	B	SE	p value
Age, years	0.006	-0.003	0.077	-0.001	0.004	0.749
Education, years	-0.010	0.006	0.089	-0.011	0.005	0.044*
Vascular risk burden	0.025	0.016	0.124	0.016	0.016	0.322
nWMH volume	-0.005	0.004	0.187	-0.007	0.004	0.066
nHippocampus volume	-0.400	0.124	0.002*	-0.442	0.141	0.003*
$K_{trans}$ of the hippocampus	0.032	0.037	0.388	0.033	0.034	0.315

Note: Multiple linear regression method using the enter method:  $R^2 = 0.267$ ,  $F(6,59) = 3.578$ ,  $p = 0.004$ .

CDR-SB: clinical dementia rating-sum of boxes; SE: standard error; WMH: white matter hyperintensity; nWMH: normalized total WMH volume; nHippocampus: normalized hippocampus volume.

\* $p < 0.05$ .

**Table 4.** Predictors of CDR-SB in the subgroup with a known APOE4 status ( $n = 35$ ).

Independent variable	Univariable regression			Multivariable regression (enter)			Multivariable regression (forward stepwise)		
	B	SE	p value	B	SE	p value	B	SE	p value
Age, years	0.004	0.004	0.347	-0.004	0.004	0.368			
Education, years	-0.010	0.007	0.176	-0.014	0.006	0.032*			
ApoE4	0.087	0.058	0.143	-0.062	0.058	0.295			
Vascular risk burden	0.008	0.021	0.713	0.010	0.018	0.569			
nWMH volume	-0.005	0.005	0.313	-0.006	0.004	0.150			
nHippocampus volume	-0.455	0.151	0.005*	-0.530	0.160	0.003*	-0.445	0.137	0.003*
$K_{trans}$ of hippocampus	0.147	0.057	0.015*	0.134	0.056	0.025*	0.142	0.050	0.008*
Vp of the inferior temporal gyrus	-0.033	0.023	0.157	-0.049	0.021	0.026*			
Vp of the globus pallidus	-0.022	0.033	0.521						
Vp of the temporal white matter	-0.003	0.012	0.803						

Note: Multiple linear regression with the forward stepwise method:  $R^2 = 0.374$ ,  $F(2, 32) = 9.559$ ,  $p = 0.001$ .

WMH: white matter hyperintensity; nWMH: normalized total WMH volume; nHippocampus: normalized hippocampus volume; APOE: apolipoprotein E; CDR-SB: clinical dementia rating-sum of boxes. Multiple linear regression with the enter method:  $R^2 = 0.540$ ,  $F(8, 26) = 3.821$ ,  $p = 0.004$ .

\* $p < 0.05$ .

status, BBB permeability was significantly higher in APOE4 carriers than in non-carriers in subjects with NC and MCI. In the subgroup analysis, we found that higher BBB permeability in the hippocampus was associated with declining cognitive function.

We did not observe a difference in BBB permeability between the NC and MCI groups in the WM regions that were examined, which is consistent with the findings of previous studies.<sup>13,29</sup> In a study on AD, no differences in BBB permeability in the WM, normally appearing WM, deep gray matter, or WM hyperintensities were observed; however, a significant increase in BBB permeability was observed in the gray matter and cortex in subjects with AD compared to normal subjects.<sup>12</sup> In a study of small vessel disease, no significant differences in BBB permeability were reported between subjects with small vessel disease and age-matched controls.<sup>30</sup>

When comparing subjects with NC and those with MCI, we observed higher BBB permeability in the left caudate nucleus of the MCI group compared with that in the NC group, which is in line with the observations of Nation et al.<sup>13</sup> However, we did not find a difference in the BBB permeability between the NC and MCI groups in any of the other deep gray matter regions, or in the chosen cortical areas.

Previous studies either did not assess BBB permeability in the hippocampus,<sup>12</sup> or reported higher BBB permeability of the hippocampus in MCI subjects than in normal controls.<sup>13,29</sup> We could not replicate the latter finding in our study group. In this study, two NC subjects were deemed to be outliers as they had markedly higher BBB permeability in the regions measured (as noted in Figure 1), the cause of which is not known. This might be because the clinical diagnosis for MCI is not equivalent to the biological definition that represents the underlying pathology itself.<sup>17,31</sup>

In our subgroup analysis, APOE4 was related to higher BBB permeability of the hippocampus. The relationship between BBB permeability and APOE4 mutation status has been investigated in animal studies.<sup>5,7</sup> However, this relationship has been touched upon only very recently in a human study.<sup>32</sup> Our finding is in line with the recent observation of increased BBB permeability in the hippocampus and parahippocampal gyrus in cognitively normal APOE4 carriers, compared to non-carriers.<sup>32</sup>

APOE4 genotype is a major risk factor for late-onset AD. APOE4 mutation is associated with earlier disease onset and more rapid disease progression of AD.<sup>33</sup> APOE4 is also a risk factor for vascular cognitive impairment, independent of AD diagnosis.<sup>34</sup>

Postmortem studies have indicated that APOE4 exacerbates the intraneuronal accumulation of amyloid beta, plaque deposition, formation of neurotoxic

amyloid beta oligomers, and severity of cerebral amyloid angiopathy.<sup>35,36</sup> Accumulating evidence suggests that APOE4 mutation influences amyloid pathology via two pathways in relation to the BBB: anatomical impairment of the BBB with accelerated pericyte loss by the presence of APOE4,<sup>5</sup> and functional impairment of the BBB by transport dysregulation.<sup>5</sup> Recent evidence also indicates a role of BBB breakdown and/or vascular dysregulation and subsequent neuroinflammation in the early stages of the AD cascade.<sup>37,38</sup>

Our findings support the idea that APOE4 mutation affects BBB integrity at the early stage of the AD cascade, in both normal individuals and MCI subjects. Thus, further exploring the interaction of APOE4 status and BBB permeability using DCE imaging may reveal how APOE4 influences AD pathology on an individual basis. We did not observe the same degree of BBB permeability change in both hemispheres despite a similar tendency, which might be partly due to the relatively small sample size and the right-handedness of the study subjects.<sup>39</sup>

Interestingly, we found a lower Vp of the inferior temporal gyrus, temporal WM, and globus pallidus in APOE4 carriers compared to non-carriers. Association between Vp and APOE4 has not been studied previously. Vp itself does not reflect BBB function, but rather represents blood plasma volume, which is associated with cerebral blood flow.<sup>40</sup> Thus, our finding is in line with a previous study, which shows decreased cerebral blood flow in APOE4 carriers in both normal and MCI subjects.<sup>41</sup>

CDR-SB as a cognitive function measure was independently correlated with BBB permeability in our subgroup analysis. Although CDR-SB was correlated only with hippocampal volume for the total population in our study, our subgroup analysis corroborated the previous finding that higher BBB permeability in the hippocampus is associated with poorer CDR scores.<sup>13</sup> BBB breakdown of the hippocampus may contribute to functional impairment of the hippocampus and other associated regions, even before the beginning of evident regional structural atrophy. Furthermore, it has been recently reported that the status of BBB breakdown can predict cognitive impairment independent of the amyloid and tau pathology.<sup>32</sup>

In our study, we chose the Patlak model because it is regarded as the most appropriate model for measuring minimal BBB leakage.<sup>11,42</sup> However, for higher values of permeability (0.3 mL/100/min), the Patlak method markedly underestimates the true permeability.<sup>43</sup> Our study results partially overlapped with the range that can be underestimated by the Patlak method. Accordingly, the true difference in the BBB permeability between the groups may have been even greater than the reported differences in this study. Hence,



our results that are statistically less convincing may be due to the mathematical model that was applied.

Our results imply that increases in BBB permeability detected using DCE imaging represent an imaging phenotype for APOE4 mutation and its expression level. In particular, by quantifying the anatomical distribution of BBB permeability, information can be obtained on local-regional variation and the actual effects of APOE4 mutation on the brain. In clinical trials, this information could be used to triage participants into subcategories that could benefit from a new drug. Furthermore, BBB permeability changes at the initial point of clinical trials may be a factor that alters the drug effects in participants. Currently, follow-up and endpoints of clinical trials for AD rely on clinical improvement, the rate of structural atrophy, and quantitative markers, such as diffusion tensor imaging parameters in some cases. However, there is a lack of imaging markers to define vascular contributions and APOE4 effects.

There are a few limitations to this study. First, the relatively small sample size may have affected the results. Second, the ROI analysis may have been both a strength and a limitation. However, whole brain analysis has its own limitations with misregistration issues with a standard template or atlas.<sup>44</sup> It would be problematic to calculate the whole brain BBB permeability when small and large vessels cannot be completely removed for analysis. As suggested in a recent review, the chosen ROIs of the WM and hippocampus are unlikely to be affected by inadvertently included vessels, as compared to the cortical gray matter.<sup>45</sup> In addition, we selected the hippocampal ROI carefully using a polygonal shape and checked the individual pixel values to avoid the inclusion of arteries and CSF, as these elements may produce spurious high  $K_{trans}$  values.<sup>46</sup> Third, our DCE imaging acquisition time was only 10 min, which is relatively short compared to recent recommendations.<sup>11</sup> For the range of small BBB permeability ( $1 - 2 \times 10^{-3} \text{ min}^{-1}$ ) as in our study, scanning longer than 15 min would be more ideal with the highest contrast-to-noise ratio.<sup>47</sup> There might have been more widespread BBB permeability changes detected with the use of a longer DCE sequence. However, in terms of clinical practice, 10 min appears to be the maximum and most reasonable acquisition time for elderly patients to minimize motion. Finally, a venous input function, which we chose in this study for VIF, can have a more dispersed and lower peak compared with an arterial input function. Many researchers have validated the use of the sagittal sinus as the VIF for model calculation, and pointed out that using the SSS results in fewer partial volume effects and inflow artifacts.<sup>48,49</sup> The sagittal sinus has a sufficiently large cross-section, from which voxels can be selected

with minimal partial volume effects. Also, venous VIFs have higher SNR and CNRs and are more representative of blood concentration than VIFs measured in the ICA, thus providing a good approximation of the VIF.<sup>11</sup> Nevertheless, choosing SSS as the vascular input function may not be optimal considering our rather fast injection protocol (2 mL/s). Although our injection protocol is relatively slow as compared to the routine DCE protocol, slow manual injection (>90 s) may be more appropriate for the accurate calculation of BBB permeability.<sup>49,50</sup>

To conclude, BBB permeability imaging using DCE MRI suggests that BBB permeability changes in the hippocampus are modulated by the presence of APOE4 mutation and correlate with cognitive function scores. Thus, BBB permeability imaging may represent a useful quantitative imaging marker to predict the degree of pathophysiology induced by APOE4 mutation.

### Funding

The author(s) disclosed receipt of the following financial support for the research, authorship, and/or publication of this article: This work was supported by the National Research Foundation of Korea (NRF) grant funded by the Korean government (MSIP) [grant number 2017R1A2B4010634] and a grant from the Korea Health Technology R&D Project through the Korea Health Industry Development Institute (KHIDI), funded by the Ministry of Health & Welfare, Republic of Korea [grant number HI18C1038].

### Declaration of conflicting interests

The author(s) declared no potential conflicts of interest with respect to the research, authorship, and/or publication of this article.

### Authors' contributions

Won-Jin Moon: design and conceptualization of the study, analysis and interpretation of the data, drafting and revising the manuscript for intellectual content.

Changmok Lim: analysis and interpretation of the data, drafting the manuscript for intellectual content.

Il Heon Ha, Yeahoon Kim: analysis and interpretation of the data, revising the manuscript for intellectual content.


Yeonsil Moon, Hee-Jin Kim, Seol-Heui Han: design and conceptualization of the study, revising the manuscript for intellectual content.

### Supplemental material

Supplemental material for this article is available online.

### ORCID iDs

Won-Jin Moon  <https://orcid.org/0000-0002-8925-7376>

Changmok Lim  <https://orcid.org/0000-0002-5245-7200>

## References

1. Arvanitakis Z, Capuano AW, Leurgans SE, et al. Relation of cerebral vessel disease to Alzheimer's disease dementia and cognitive function in elderly people: a cross-sectional study. *Lancet Neurol* 2016; 15: 934–943.
2. Grinberg LT and Thal DR. Vascular pathology in the aged human brain. *Acta Neuropathol* 2010; 119: 277–290.
3. Nelson AR, Sweeney MD, Sagare AP, et al. Neurovascular dysfunction and neurodegeneration in dementia and Alzheimer's disease. *Biochim Biophys Acta* 2016; 1862: 887–900.
4. Zlokovic BV. The blood-brain barrier in health and chronic neurodegenerative disorders. *Neuron* 2008; 57: 178–201.
5. Halliday MR, Rege SV, Ma Q, et al. Accelerated pericyte degeneration and blood-brain barrier breakdown in apolipoprotein E4 carriers with Alzheimer's disease. *J Cereb Blood Flow Metab* 2016; 36: 216–227.
6. Lim YY, Kalinowski P, Pietrzak RH, et al. Association of beta-amyloid and apolipoprotein E epsilon4 with memory decline in preclinical Alzheimer disease. *JAMA Neurol* 2018; 75: 488–494.
7. Alata W, Ye Y, St-Amour I, et al. Human apolipoprotein E varepsilon4 expression impairs cerebral vascularization and blood-brain barrier function in mice. *J Cereb Blood Flow Metab* 2015; 35: 86–94.
8. Ujiie M, Dickstein DL, Carlow DA, et al. Blood-brain barrier permeability precedes senile plaque formation in an Alzheimer disease model. *Microcirculation* 2003; 10: 463–470.
9. Sengillo JD, Winkler EA, Walker CT, et al. Deficiency in mural vascular cells coincides with blood-brain barrier disruption in Alzheimer's disease. *Brain Pathol* 2013; 23: 303–310.
10. Bowman GL, Kaye JA, Moore M, et al. Blood-brain barrier impairment in Alzheimer disease: stability and functional significance. *Neurology* 2007; 68: 1809–1814.
11. Thrippleton MJ, Backes WH, Sourbron S, et al. Quantifying blood-brain barrier leakage in small vessel disease: review and consensus recommendations. *Alzheimers Dement* 2019; 15: 840–858.
12. van de Haar HJ, Burgmans S, Jansen JF, et al. Blood-brain barrier leakage in patients with early Alzheimer disease. *Radiology* 2016; 281: 527–535.
13. Nation DA, Sweeney MD, Montagne A, et al. Blood-brain barrier breakdown is an early biomarker of human cognitive dysfunction. *Nat Med* 2019; 25: 270–276.
14. Montagne A, Zhao Z and Zlokovic BV. Alzheimer's disease: a matter of blood-brain barrier dysfunction? *J Exp Med* 2017; 214: 3151–3169.
15. Park M, Moon WJ, Moon Y, et al. Region-specific susceptibility change in cognitively impaired patients with diabetes mellitus. *PLoS One* 2018; 13: e0205797.
16. McKhann G, Drachman D, Folstein M, et al. Clinical diagnosis of Alzheimer's disease: report of the NINCDS-ADRDA work group under the auspices of department of health and human services task force on Alzheimer's disease. *Neurology* 1984; 34: 939–944.
17. Petersen RC, Smith GE, Waring SC, et al. Mild cognitive impairment: clinical characterization and outcome. *Arch Neurol* 1999; 56: 303–308.
18. Taheri S, Gasparovic C, Shah NJ, et al. Quantitative measurement of blood-brain barrier permeability in human using dynamic contrast-enhanced MRI with fast T1 mapping. *Magn Reson Med* 2011; 65: 1036–1042.
19. Wardlaw JM, Smith EE, Biessels GJ, et al. Neuroimaging standards for research into small vessel disease and its contribution to ageing and neurodegeneration. *Lancet Neurol* 2013; 12: 822–838.
20. Lee JS, Kim C, Shin JH, et al. Machine learning-based individual assessment of cortical atrophy pattern in Alzheimer's disease spectrum: development of the classifier and longitudinal evaluation. *Sci Rep* 2018; 8: 4161.
21. Jeon S, Yoon U, Park J-S, et al. Fully automated pipeline for quantification and localization of white matter hyperintensity in brain magnetic resonance image. *Int J Imag Syst Technol* 2011; 21: 193–200.
22. Jung NY, Cho H, Kim YJ, et al. The impact of education on cortical thickness in amyloid-negative subcortical vascular dementia: cognitive reserve hypothesis. *Alzheimers Res Ther* 2018; 10: 103.
23. Fischl B, Salat DH, Busa E, et al. Whole brain segmentation: automated labeling of neuroanatomical structures in the human brain. *Neuron* 2002; 33: 341–355.
24. Guo C, Ferreira D, Fink K, et al. Repeatability and reproducibility of FreeSurfer, FSL-SIENAX and SPM brain volumetric measurements and the effect of lesion filling in multiple sclerosis. *Eur Radiol* 2019; 29: 1355–1364.
25. Sundar H, Shen D, Biros G, et al. Robust computation of mutual information using spatially adaptive meshes. *Med Image Comput Comput Assist Interv* 2007; 10: 950–958.
26. Desikan RS, Segonne F, Fischl B, et al. An automated labeling system for subdividing the human cerebral cortex on MRI scans into gyral based regions of interest. *Neuroimage* 2006; 31: 968–980.
27. Mattsson N, Palmqvist S, Stomrud E, et al. Staging beta-amyloid pathology with amyloid positron emission tomography. *JAMA Neurol* 2019; 76: 1319–1329.
28. Insel PS, Mormino EC, Aisen PS, et al. Neuroanatomical spread of amyloid beta and tau in Alzheimer's disease: implications for primary prevention. *Brain Commun* 2020; 2: fcaa007.
29. Montagne A, Barnes SR, Sweeney MD, et al. Blood-brain barrier breakdown in the aging human hippocampus. *Neuron* 2015; 85: 296–302.
30. Zhang CE, Wong SM, van de Haar HJ, et al. Blood-brain barrier leakage is more widespread in patients with cerebral small vessel disease. *Neurology* 2017; 88: 426–432.
31. Jack CR, Jr., Bennett DA, Blennow K, et al. NIA-AA research framework: toward a biological definition of Alzheimer's disease. *Alzheimers Dement* 2018; 14: 535–562.
32. Montagne A, Nation DA, Sagare AP, et al. APOE4 leads to blood-brain barrier dysfunction predicting cognitive decline. *Nature* 2020; 581: 71–76.

33. Sando SB, Melquist S, Cannon A, et al. APOE epsilon 4 lowers age at onset and is a high risk factor for Alzheimer's disease; a case control study from central Norway. *BMC Neurol* 2008; 8: 9.
34. Mirza SS, Saeed U, Knight J, et al. APOE epsilon4, white matter hyperintensities, and cognition in Alzheimer and Lewy body dementia. *Neurology* 2019; 93: e1807–e1819.
35. Ellis RJ, Olichney JM, Thal LJ, et al. Cerebral amyloid angiopathy in the brains of patients with Alzheimer's disease: the CERAD experience, Part XV. *Neurology* 1996; 46: 1592–1596.
36. Polvikoski T, Sulkava R, Haltia M, et al. Apolipoprotein E, dementia, and cortical deposition of beta-amyloid protein. *N Engl J Med* 1995; 333: 1242–1247.
37. Janelidze S, Mattsson N, Stomrud E, et al. CSF biomarkers of neuroinflammation and cerebrovascular dysfunction in early Alzheimer disease. *Neurology* 2018; 91: e867–e877.
38. Bowman GL, Dayon L, Kirkland R, et al. Blood-brain barrier breakdown, neuroinflammation, and cognitive decline in older adults. *Alzheimers Dement* 2018; 14: 1640–1650.
39. Shu XJ, Xue L, Liu W, et al. More vulnerability of left than right hippocampal damage in right-handed patients with post-traumatic stress disorder. *Psychiatry Res* 2013; 212: 237–244.
40. Li Y, Li M, Zuo L, et al. Compromised blood-brain barrier integrity is associated with total magnetic resonance imaging burden of cerebral small vessel disease. *Front Neurol* 2018; 9: 221.
41. Michels L, Warnock G, Buck A, et al. Arterial spin labeling imaging reveals widespread and A-beta-independent reductions in cerebral blood flow in elderly apolipoprotein epsilon-4 carriers. *J Cereb Blood Flow Metab* 2016; 36: 581–595.
42. Heye AK, Thrippleton MJ, Armitage PA, et al. Tracer kinetic modelling for DCE-MRI quantification of subtle blood-brain barrier permeability. *Neuroimage* 2016; 125: 446–455.
43. Cramer SP and Larsson HB. Accurate determination of blood-brain barrier permeability using dynamic contrast-enhanced T1-weighted MRI: a simulation and in vivo study on healthy subjects and multiple sclerosis patients. *J Cereb Blood Flow Metab* 2014; 34: 1655–1665.
44. Snook L, Plewes C and Beaulieu C. Voxel based versus region of interest analysis in diffusion tensor imaging of neurodevelopment. *Neuroimage* 2007; 34: 243–252.
45. Raja R, Rosenberg GA and Caprihan A. MRI measurements of Blood-Brain Barrier function in dementia: a review of recent studies. *Neuropharmacology* 2018; 134: 259–271.
46. Lim CM and Moon WJ. Methodologic concerns on the reported values for assessing permeability of the blood-brain barrier in the hippocampus. *AJNR Am J Neuroradiol* 2019; 40: E65–E66.
47. Barnes SR, Ng TS, Montagne A, et al. Optimal acquisition and modeling parameters for accurate assessment of low K<sub>trans</sub> blood-brain barrier permeability using dynamic contrast-enhanced MRI. *Magn Reson Med* 2016; 75: 1967–1977.
48. Ewing JR, Knight RA, Nagaraja TN, et al. Patlak plots of Gd-DTPA MRI data yield blood-brain transfer constants concordant with those of 14C-sucrose in areas of blood-brain opening. *Magn Reson Med* 2003; 50: 283–292.
49. Wong SM, Jansen JFA, Zhang CE, et al. Measuring subtle leakage of the blood-brain barrier in cerebrovascular disease with DCE-MRI: test-retest reproducibility and its influencing factors. *J Magn Reson Imaging* 2017; 46: 159–166.
50. Wang H, Golob EJ and Su MY. Vascular volume and blood-brain barrier permeability measured by dynamic contrast enhanced MRI in hippocampus and cerebellum of patients with MCI and normal controls. *J Magn Reson Imaging* 2006; 24: 695–700.